THE JOURNAL OF PHYSICAL CHEMISTRY Letters

Letter

pubs.acs.org/JPCL

Energy Level Alignment and Charge Carrier Mobility in Noncovalently Functionalized Graphene

Liping Chen,*[,†] Linjun Wang,[†] Zhigang Shuai,[‡] and David Beljonne[†]

[†]Laboratory for Chemistry of Novel Materials, University of Mons, Place du Parc 20, B-7000 Mons, Belgium

[‡]MOE Key Laboratory of Organic OptoElectronics and Molecular Engineering, Department of Chemistry, Tsinghua University, 100084 Beijing, People's Republic of China

Supporting Information

ABSTRACT: Density functional theory calculations have been performed to assess the electronic structure of graphene overlaid with a monolayer of electro-active conjugated molecules, being either electron donors or electron acceptors. Such a noncovalent functionalization results in a work function modification that scales with the amount of electron transfer from or to graphene, in line with the formation of an interfacial dipole. The charge transfer is accompanied by a pinning of the donor HOMO/acceptor LUMO around the Fermi level and a shift in the vacuum level. The use of the Boltzmann transport equation combined with the deformation potential theory shows that large charge carrier mobilities are maintained upon noncovalent functionalization of graphene, thereby suggesting that molecular doping is an attractive approach to design conductive graphene electrodes with tailored work function.

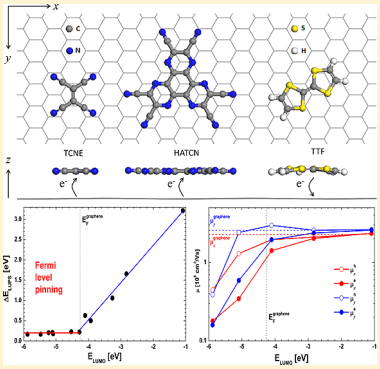

SECTION: Surfaces, Interfaces, Porous Materials, and Catalysis

Graphene, a single layer of graphite, was first obtained by Novoselov and co-workers.[1] Due to its special honeycomb structure, the valence band (VB) and the conduction band (CB) intersect at the Dirac point, and the energy-momentum dispersion is essentially linear around the Dirac point. This results in the excellent electronic properties of graphene, especially the ballistic charge transport with extremely high charge carrier mobility up to 2×10^5 $cm^2/(V\ s)$.[2] Therefore, graphene-based nanoelectronics have been considered as a promising alternative to conventional silicon-based microelectronics.[3−5] Due to the intersection of VB and CB, the Fermi level in pristine graphene goes exactly across the Dirac point. By shifting the Fermi level relative to the Dirac point, the carrier type and concentration in graphene can be controlled through electrical doping with an external electric field[6,7] or chemical doping with different atoms and/or molecules.[8,9]

It has been shown that graphene can be n-doped by depositing alkali metal atoms on the surface.[10] However, the carrier mobility of graphene can be significantly reduced in the presence of the charged impurities. After doping with N or B atoms, graphene becomes n-type or p-type, respectively.[11,12] Wei and co-workers show that there are many ripples in the graphene sheet as a result of N-doping, and the resulting mobility of N-doped graphene is rather low compared to undoped graphene, with values in the range 200−450 $cm^2/(V\ s)$.[12] The electronic properties of graphene can also be tuned by chemical modification like partially or fully hydrogenation and fluorination.[13,14] However, due to the strong covalent bond of C−H and C−F, the sp^2 hybridization of carbon atoms is disrupted, and the induced structural defects and chemical impurities can easily destroy the excellent properties of graphene, especially the high carrier mobility. Calculations based on density functional theory (DFT) show that the charge mobility of hydrogenated or fluorinated graphene drops dramatically compared to graphene.[15]

On the contrary, noncovalent functionalization, through physisorption of electron withdrawing/donating molecules on the graphene surface, has been reported to be a simple and effective scheme to nondestructively dope graphene.[16,17] Here, the doping is achieved by charge transfer between graphene and the molecular dopants. Since the weak van de Waals (vdW) interactions dominate in noncovalent functionalization, graphene does not show strong structural deformation, and in most cases the doping is reversible. Recently, Chen et al.[16] have used a strong electron acceptor, namely, tetrafluoro-tetracyanoquinodimethane (F4-TCNQ), to modify the graphene surface and have found that graphene is effectively p-doped by giving electrons to F4-TCNQ. Voggu and co-workers have demonstrated that graphene can be p-doped and n-doped by a molecular donor tetrathiafulvalene (TTF) and a molecular acceptor tetracyanoethylene (TCNE), respectively.[17] Theoretical calculations can help gaining a better understanding of the noncovalent interaction between graphene and the molecular

Received: May 16, 2013
Accepted: June 13, 2013
Published: June 13, 2013

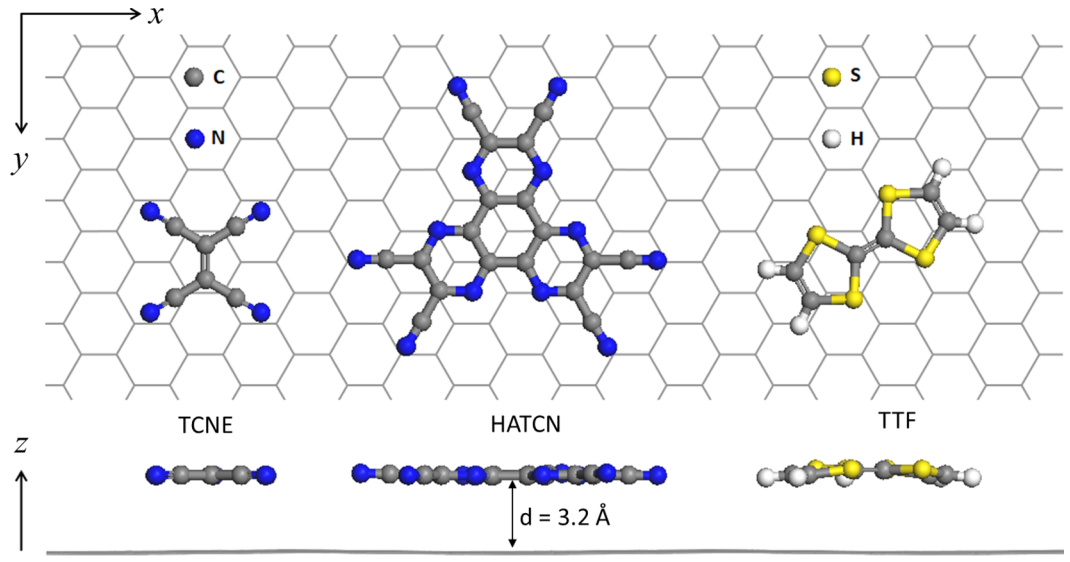

Figure 1. Top and side views of the most stable configurations of TCNE, HATCN, and TTF adsorbed on graphene. x−y plane is the graphene plane, and z is normal to the graphene plane.

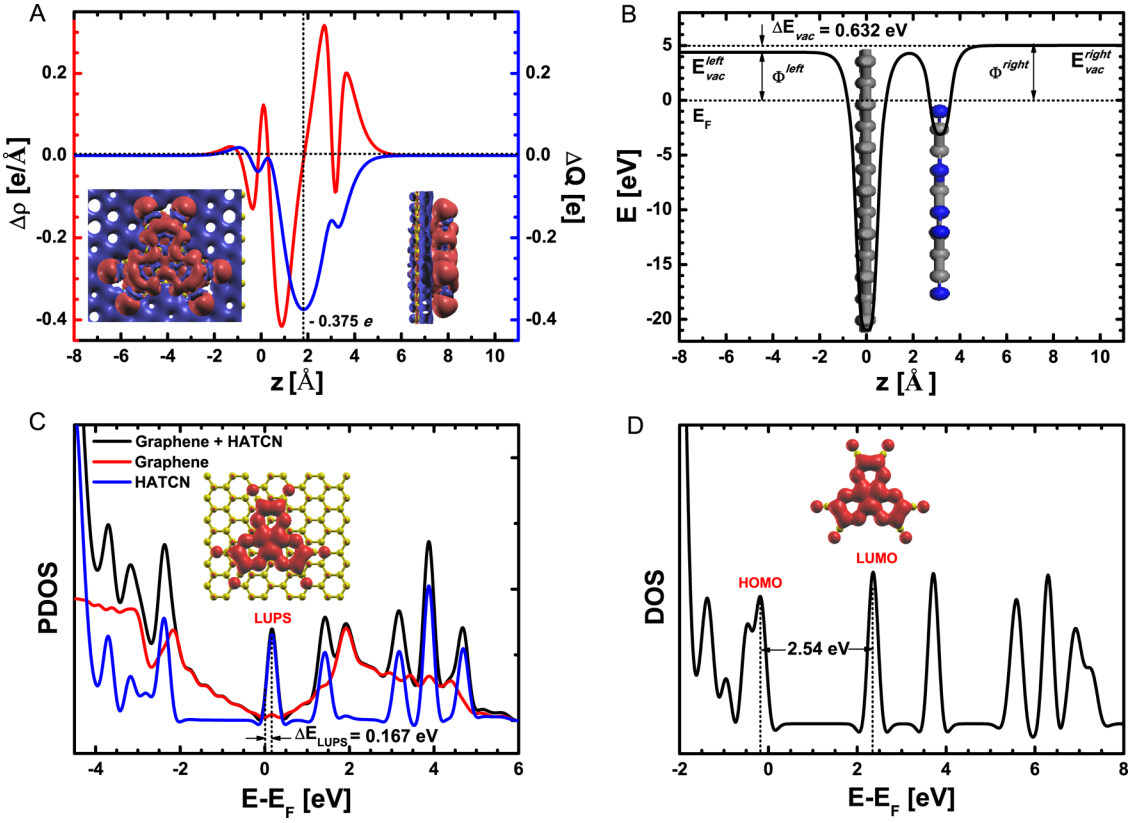

Figure 2. Properties of HATCN adsorbed on graphene. (A) Plane-averaged DCD $\Delta\rho(z)$, charge transfer amount $\Delta Q(z)$, and top and side views of the 0.001 Å^{-3} DCD isosurface (in the inset). The electron accumulation (depletion) region in the DCD isosurface is indicated by red (blue) color. (B) Plane-averaged potential energy $E(z)$. (C) DOS of the adsorbed system, PDOS of graphene and HATCN, and LDOS of the LUPS peak. (D) DOS of a single HATCN molecule and LDOS of the LUMO peak.

dopants. Investigations based on DFT have been carried out on graphene functionalized with typical electron donors and acceptors, such as TTF,[18−20] TCNE,[19−21] and F4-TCNQ.[18,22] The amount of charge transfer and the work function modification have been obtained from these calculations. However, so far, there has been neither systematic investigation on the relationship between charge transfer process and the energy level alignment at the graphene−molecule interface, nor numerical calculations on the influence of functionalizing graphene with electro-active molecules on the resulting charge carrier mobility.

In this work, we perform first-principles calculations on noncovalently functionalized graphene with TCNE, TTF, and hexaazatriphenylene-hexacarbonitrile (HATCN) (see Figure

dx.doi.org/10.1021/jz4010174 | J. Phys. Chem. Lett. 2013, 4, 2158−2165

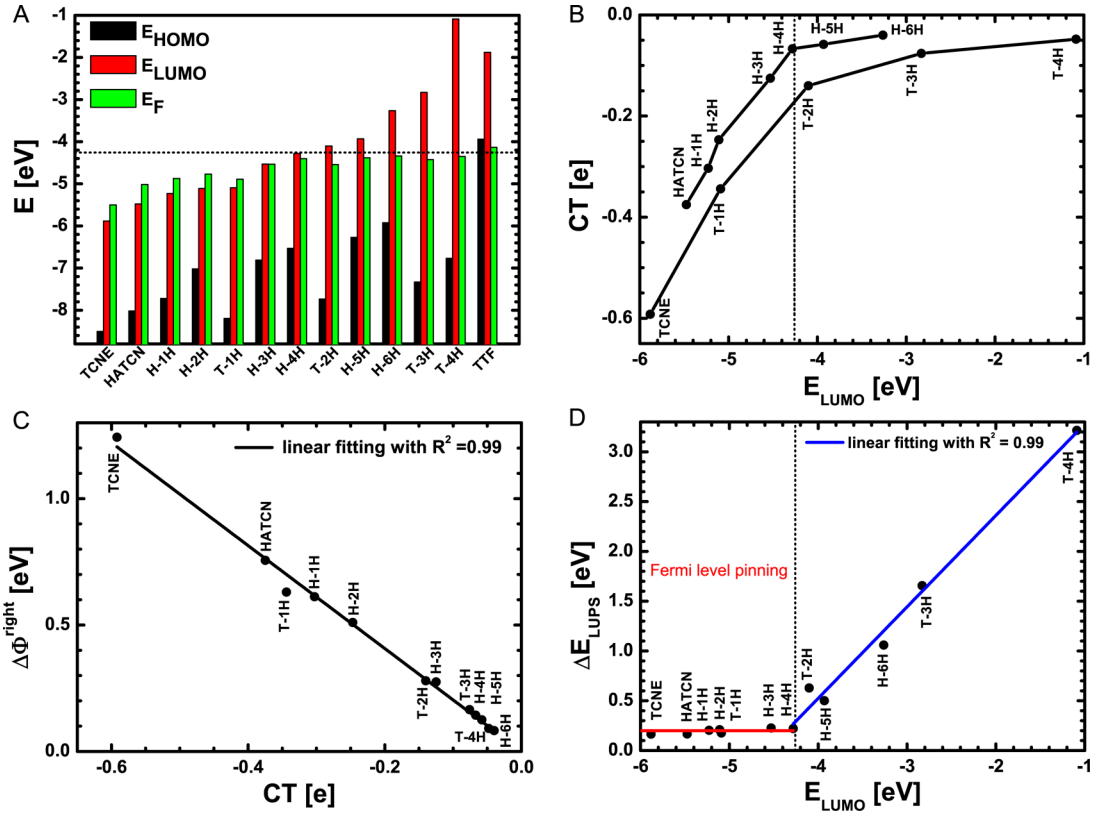

Figure 3. (A) Molecular HOMO and LUMO levels and Fermi level of the adsorbed systems. (B) Relationship between the amount of charge transfer amount within the $4\sqrt{3}$ * 6 supercell and the molecular LUMOs. (C) Linear relationship between the work function modification of graphene and the amount of charge transfer within the $4\sqrt{3}$ * 6 supercell. (D) Relationship between ΔE_{LUPS} and the molecular LUMOs. While the red line shows the Fermi level pinning with ΔE_{LUPS} = 0.2 eV, the blue line shows the linear relationship between ΔE_{LUPS} and E_{LUMO}. Dotted lines in A, B, and D indicate the graphene Fermi level with the vacuum level shifted to zero.

1). While the presence of CN groups conveys a strong electron acceptor character to TCNE and HATCN, TTF behaves as an electron donor owing to its electron-rich sulfur atoms. In order to systematically investigate the interaction between graphene and various molecular dopants, we design two series of model "gedanken" systems obtained by gradually replacing the CN groups of TCNE and HATCN with H atoms (see Figure S1). They are hereafter referred as T-nH (n = 1, 2, 3, and 4) and H-nH (n = 1, 2, 3, 4, 5, and 6) according to the number of H atoms. In the following, we investigate the adsorption geometry, the amount of charge transfer, the density of states, the work function modification, the energy level alignment, as well as the carrier mobility of graphene covered with a monolayer of the electro-active molecules.

We have considered various initial configurations for the molecules adsorbed face to face on graphene. Our calculations show that the energy difference between different configurations is small. Therefore, we only consider for further investigations the most stable configurations that are in line with previous results (see Figure 1).[18,20,21] Due to its large conjugated core, HATCN adopts AB-stacking as in graphite at low coverage.[23] While TCNE and HATCN keep their planar geometries when adsorbed on graphene, the TTF core slightly bends toward graphene, in line with investigations by Sun et al.[18] For all adsorbed systems, there is no significant distortion of graphene with the rumpling less than 0.1 Å; the mean distance between graphene and the molecule is around 3.2 Å. The adsorption energy is calculated as $E_{ads} = E_{graphene} + E_{molecule} - E_{graphene+molecule}$, where $E_{graphene+molecule}$ is the energy of the molecular functionalized graphene, and $E_{graphene}$ and $E_{molecule}$ are the energies of the isolated graphene and molecule with their geometries frozen in the optimized adsorbed system. As shown in Table S1, due to the strong electrostatic interaction of the CN groups and the sizable $\pi-\pi$ interaction with the conjugated core, the adsorption energy of HATCN is the highest among all molecular dopants investigated here.

In order to assess the electronic fingerprint of noncovalent functionalization on graphene, we have computed the differential charge density (DCD) due to the molecular adsorption. The DCDs for HATCN adsorbed on graphene are depicted in the inset of Figure 2A. As expected from its withdrawing character, HATCN gains electron when adsorbed on graphene. In order to quantify the amount of charge transfer between graphene and the molecule, the plane-averaged DCD $\Delta\rho(z)$ is obtained by integrating the DCD over the $x-y$ plane. Accordingly, for a plane located at distance z normal to the graphene plane, the amount of charge transfer is calculated as $\Delta Q(z) = \int_{-\infty}^{z} \Delta\rho(z')dz'$. The plane-averaged DCD $\Delta\rho(z)$ and the amount of charge transfer $\Delta Q(z)$ for HATCN adsorbed on graphene, plotted in Figure 2A, show that the charge transfer reaches a maximum value of -0.375 e at the graphene–molecule interface (e is the elementary charge of an electron).

Steps in potential energy induced by changes in charge density can be calculated by solving the Poisson equation $\nabla^2 E(z) = (e/\varepsilon_0)\Delta\rho(z)$, where $E(z)$ is the plane-averaged potential energy and ε_0 is the vacuum permittivity. Figure 2B indicates a shift in vacuum level when going from one side of the graphene plane to the other. The vacuum level shift is

dx.doi.org/10.1021/jz4010174 | J. Phys. Chem. Lett. 2013, 4, 2158–2165

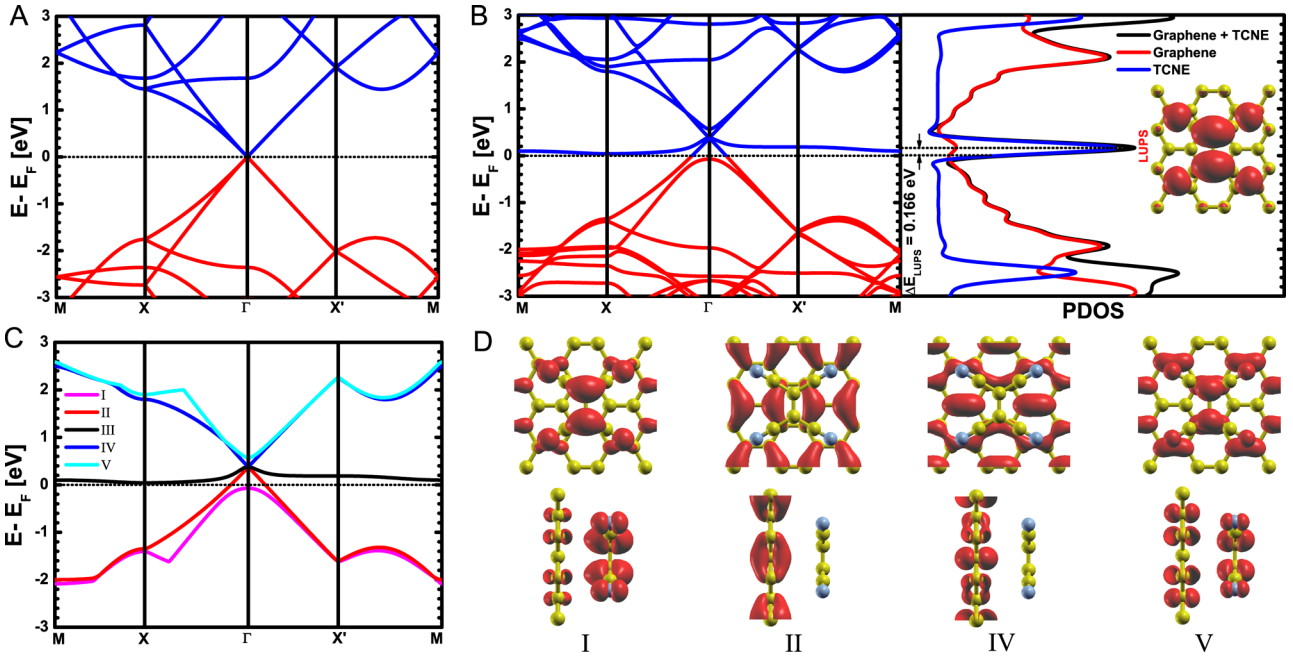

Figure 4. (A) Band structures of the $2\sqrt{3}$ * 3 supercell graphene. (B) Band structures and PDOS of the $2\sqrt{3}$ * 3 supercell graphene noncovalently functionalized with TCNE. (C) Five frontier bands around the Fermi level in B labeled as I, II, III, IV, and V. (D) Top and side views of the 0.015 $Å^{-3}$ charge density isosurface at Γ point for the bands labeled as I, II, IV, and V in C.

calculated as $\Delta E_{vac} = E_{vac}^{right} - E_{vac}^{left}$, where E_{vac}^{right} (E_{vac}^{left}) is the vacuum level on the right (left) side of graphene with (without) overlaying molecules. For HATCN, E_{vac}^{right} is shifted up relatively to E_{vac}^{left} by ΔE_{vac} = 0.632 eV. As the vacuum level shifts, the work function (Φ), defined as the energy difference between the vacuum level and the Fermi level, is modified accordingly. The work function modification of graphene on both sides is calculated as $\Delta\Phi^{left(right)} = \Phi^{left(right)} - \Phi_{graphene}$, where $\Phi_{graphene}$ is the work function of pristine graphene. We can get $\Delta\Phi^{right} = \Delta\Phi^{left} + \Delta E_{vac}$ from Figure 2B. Our calculation shows that $\Delta\Phi^{left}$ is significant with a value of 0.124 eV after the adsorption of HATCN. This is in contrast with previous investigations of self-assembled monolayers (SAMs) on noble metals like gold and silver, where the work function on the metal side remains unchanged after the adsorption of SAMs on the other side of the metal.[24] Because of the reduced electron density in the graphene layer, the work function of graphene is increased by 0.756 eV in the presence of the HATCN electron acceptor.

The density of states (DOS) for HATCN functionalized graphene and the projected density of states (PDOS) onto graphene and HATCN, shown in Figure 2C, reveal the presence of a peak around the Fermi level in the DOS; analysis of the PDOS shows that HATCN provides the main contribution to this peak. To gain further insight, we next analyze the local density of states (LDOS) by integrating it in an energy window (±0.1 eV) around the peak (as shown in the inset of Figure 2C). The LDOS displays the typical features of the lowest unoccupied molecular orbital (LUMO) of HATCN (see Figure 2D), thus the peak close to the Fermi level is associated with the lowest unoccupied π state (LUPS) in the adsorbed system. In other words, the LUMO of HATCN is pinned around the Fermi level upon adsorption on graphene. The phenomenon of Fermi level pinning (FLP) has been widely observed for SAMs on Au.[24,25] We define the energy difference between the peak and the Fermi level as ΔE_{LUPS}, which is 0.167 eV for HATCN.

As indicated before, the CN groups considerably contribute to the high electron affinity of HATCN and, as a result, play an important role in the charge transfer from graphene. By replacing the CN groups of HATCN with H atoms, we obtain six model gedanken molecules with different electron withdrawing ability. From Table S1, we can see that as the number of the CN group decreases, the adsorption energy, the vacuum level shift, the work function modification, and the amount of charge transfer all reduce in a monotonous way. For H-6H with no CN group, the adsorption energy is as high as 1.129 eV due to $\pi-\pi$ and CH$-\pi$ interactions.[26] However, the amount of charge transfer is almost zero, and the vacuum level shift and the work function modification are negligible. The molecular LUMO is no longer pinned around the Fermi level and ΔE_{LUPS} is as high as 1.060 eV (see Figure S2). Therefore, the FLP is dominated by the charge transfer mechanism.

In Figure 3A, we schematically summarize the energy of molecular highest occupied molecular orbital (HOMO) and LUMO and the corresponding Fermi level of the adsorbed systems, and compare these with the graphene Fermi level. If the molecular LUMO is lower than the graphene Fermi level, as found for TCNE, T-1H, HATCN, and H-1H−H-4H, electron density drifts from graphene to the adsorbed molecules, the Fermi level is downshifted, and the work function is increased. The larger the energy mismatch between the molecular LUMO and the graphene Fermi level, the larger the Fermi level shift and the work function modification. Similarly, if the molecular HOMO is higher than the graphene Fermi level, such as for TTF, electronic density is transferred from the adlayer to graphene, the Fermi level is upshifted, and the work function is decreased. If the graphene Fermi level lies between the molecular HOMO and LUMO, as is the case for T-2H−T-4H, H-5H, and H-6H, there is negligible charge transfer and work function modification. Therefore, a simple calculation of the molecular HOMO and LUMO levels of the electro-active molecules provides a first hint on whether these are able to p-

dx.doi.org/10.1021/jz4010174 | J. Phys. Chem. Lett. 2013, 4, 2158−2165

or n-dope graphene. As shown in Figure 3B, the amount of charge transfer depends strongly on the molecular LUMOs for the TCNE and HATCN series. For all adsorbed systems, the work function modification is found to be linearly dependent on the amount of charge transfer (see Figure 3C). This can be understood according to the Helmholtz equation $\Delta\Phi = -e\mu_z/(\varepsilon_0 A)$, which states that the work function modification $\Delta\Phi$ is proportional to the dipole moment per surface area μ_z/A. Since the average distance between the molecule and graphene is almost constant, the dipole moment is linear with the amount of charge transfer. Therefore, the work function modification is controlled by charge transfer at the interface. As shown in Figure 3D, for the systems with charge transfer, the molecular LUMOs are pinned around the Fermi level with a constant ΔE_{LUPS} of ca. 0.2 eV; in the absence of significant charge transfer, ΔE_{LUPS} is large and increases linearly with the molecular LUMO. The FLP is also observed in TTF-functionalized graphene with the HOMO of TTF pinned around the Fermi level (see Figure S3).

It is well-known that conventional DFT functionals tend to underestimate energy bandgaps. Recently, the screened exchange hybrid exchange-correlation functional HSE[27,28] has been shown to yield electronic structure for molecules and solids in closer agreement with experiment.[29] Therefore, we have also applied the hybrid functional HSE06[28] with dispersion correction[30] (HSE-D) in order to gauge the robustness of the findings above based on PBE-D (see Methods). As expected, the HSE-D molecular band gaps are larger than the corresponding PBE-D values. For example, the band gap of HATCN increases from 2.54 to 3.73 eV. Yet, the FLP phenomenon is still observed with ΔE_{LUPS} = 0.181 eV (see Figure S4), which suggests that the present conclusions are weakly method sensitive.

The electronic band structures of graphene and non-covalently functionalized graphene with TCNE series are depicted in Figures 4 and S5. The intersection of the VB and CB at the Γ symmetry point (instead of the K point) arises from band folding of the $2\sqrt{3}$ * 3 graphene supercell, which also results in two degenerate VB (CB) frontier electronic bands with linear energy-momentum dispersion around the Dirac point. For the systems with negligible charge transfer, such as graphene functionalized with T-*n*H (*n* = 2, 3 and 4), the linear dispersion relationship is preserved around the Fermi level, while a flat band associated with the quasi noninteracting molecules appears far away from the Fermi level. However, for the system with significant charge transfer, especially graphene functionalized with TCNE in Figure 4B, the Fermi level is shifted 0.37 eV below the Dirac point due to the partial charge transfer from graphene to TCNE, and a flat band appears just above the Fermi level. This is mostly contributed by the LUMO of the TCNE molecules, as evidenced by the analysis of the corresponding PDOS and LDOS (see Figure 4B). Since VB and CB around the Fermi level play an important role in charge carrier transport, we further analyze the five frontier bands of TCNE functionalized graphene and plot their charge densities at the Γ point in Figure 4C and 4D. As discussed above, the flat band labeled as III arises from the LUMO of TCNE. For bands II and IV with a linear dispersion relationship as in pristine graphene, the charge density is primarily delocalized over graphene. Bands I and V, which deviate from the linear dispersion relationship, feature charge densities that are distributed over the whole system due to the interaction between TCNE and graphene.

The Boltzmann transport equation coupled with the deformation potential (DP) theory is next applied to calculate the room temperature (300 K) charge carrier mobility of pristine and doped (by TCNE and its variants) graphene (see Methods).[31] The DP constant E_1, the elastic constant *C* and the hole (electron) mobility $\mu^{h(e)}$ along *x* and *y* for the investigated systems are listed in Table 1. The calculated hole and electron

Table 1. The DP Constant E_1, the Elastic Constant *C* and the Hole (Electron) Mobility $\mu^{h(e)}$ along *x* and *y* for the $2\sqrt{3} \times 3$ Supercell of Pristine Graphene and Noncovalently Functionalized Graphene by TCNE Series

	direction	E_1 (eV)	C (J/m^2)	μ^h (cm^2/(V s))	μ^e (cm^2/(V s))
graphene + TCNE	*x*	2.492	349.42	4.46E5	1.79E5
	y	2.760	400.79	3.88E5	1.59E5
graphene + T-1H	*x*	3.698	346.01	1.29E6	3.44E5
	y	2.844	391.78	2.40E6	5.88E5
graphene + T-2H	*x*	5.448	344.57	1.95E6	1.41E6
	y	4.830	391.22	2.97E6	1.94E6
graphene + T-3H	*x*	5.418	344.48	2.10E6	2.02E6
	y	5.196	383.73	2.57E6	2.37E6
graphene + T-4H	*x*	5.190	344.16	2.34E6	2.35E6
	y	5.192	381.79	2.62E6	2.58E6
graphene	*x*	5.316	345.24	2.27E6	2.26E6
	y	5.280	381.19	2.57E6	2.53E6
graphene[a]	*x*	5.316	345.24	1.17E5	1.13E5
	y	5.280	381.19	1.33E5	1.26E5
graphene + TCNE[b]	*x*	2.492	349.42	4.46E5	4.79E5
	y	2.760	400.79	3.88E5	4.26E5

[a]Pure charge doping of graphene by shifting the Fermi level 0.37 eV below the Dirac point. [b]Neglecting the contribution from the TCNE-related flat band.

mobility of graphene, in the range 2.2−2.6 × 10^6 cm^2/(V s), is in reasonable agreement with the experimental value of 2 × 10^5 cm^2/(V s).[2] Compared with pristine graphene, the elastic constant *C* is almost unchanged for all the adsorbed systems since the interaction between graphene and the molecule is weak and the induced structural deformation in graphene is small. In the absence of significant charge transfer, such as graphene functionalized with T-*n*H (*n* = 2, 3, and 4), the band structure around the Fermi level in Figure S5 is similar to that in Figure 4A. Therefore, the DP constant E_1 and as a result the mobility are almost the same as in pristine graphene. By contrast, upon charge flow from graphene to the electro-active molecules (in particular, in the case of graphene functionalized with TCNE), although the DP constant E_1 is systematically reduced, both hole and electron mobility decrease, the effect being more pronounced for the electron mobility. To gain deeper insight on how noncovalent functionalization influences charge transport, we have investigated the charge carrier mobility in graphene: (i) in the hypothetical case of "pure charge doping", mimicked here by shifting the Fermi level 0.37 eV below the Dirac point (as in TCNE doped graphene); and (ii) while excluding in the Boltzmann mobility calculations the contribution from the TCNE-related flat band. The results reported in Table 1 show that (i) a pure charge doping scenario would yield hole and electron mobility that are 1 order of magnitude less than the pristine graphene results, thus the shift in Fermi level energy has a negative impact on charge carrier mobility; (ii) both hole and electron mobility of TCNE doped

dx.doi.org/10.1021/jz4010174 | J. Phys. Chem. Lett. 2013, 4, 2158−2165

graphene without the flat band are roughly a factor of 4 larger than the pure charge doped graphene results, showing that the negative impact of Fermi level shift on charge carrier mobility is partly compensated by the reduced electron−phonon coupling DP value due to the adlayer; (iii) the presence of a flat band localized on the TCNE molecules has a negligible impact on hole mobility (as that band lies well above the Fermi level) but is responsible for a further drop by a factor ∼2.5 of the electron mobility, implying that the weakly dispersive TCNE-derived LUMO bands in Figure 4B feed an additional electron trapping mechanism. Overall, the charge carrier mobility in TCNE-doped graphene thus results from the interplay between antagonist effects: while the doping-induced shift in Fermi energy away from the Dirac point is detrimental to both hole and electron mobility, this is partly counterbalanced by the smaller DP constant computed for the decorated graphene sheets; for electrons, an extra contribution associated with trapping further reduces the mobility. Yet, compared with pristine graphene, the mobility of TCNE functionalized graphene (which displays the largest amount of charge transfer among the systems investigated here) is reduced by *only* 1 order of magnitude. As shown in Figure 5, the higher the molecular LUMO, the smaller the amount of charge transfer and thus the closer the mobility to that of graphene. Therefore, it is in principle possible to achieve a compromise between the work function modification and the charge carrier mobility in noncovalently functionalized graphene, which paves the way toward the use of molecular doping as a viable strategy for conductive graphene electrodes.

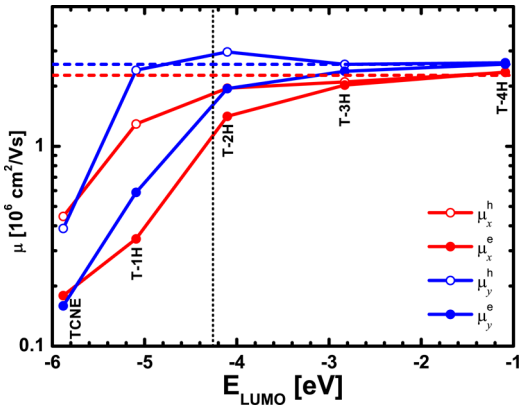

Figure 5. Relationship between the molecular LUMO and the hole (electron) mobility $\mu^{h(e)}$ along x and y for the $2\sqrt{3} * 3$ supercell of graphene noncovalently functionalized with TCNE derivatives. The red and blue dash lines are the mobilities of pristine graphene along x and y, respectively. The dotted line indicates the graphene Fermi level with the vacuum level shifted to zero.

In summary, we have investigated the changes in the electronic structure of graphene upon physical adsorption of electro-active molecules with varying donor/acceptor character from first-principles DFT calculations. Our calculations show that noncovalent functionalization of graphene results in a partial charge transfer whose magnitude depends on the energetic position of the dopant molecular frontier orbitals. This reshuffling in the electronic density yields a change in the work function that varies linearly with the amount of charge transfer. The interfacial charge transfer is accompanied by a pinning of the donor HOMO/acceptor LUMO molecular frontier orbital that appears as flat bands around the Fermi level. We have also calculated the charge carrier mobility of noncovalently functionalized graphene by applying the Boltzmann transport equation and the deformation potential theory. We find that in the absence of charge transfer from or to graphene, the carrier mobility is almost the same as that of graphene. In the n-doped case, both hole and electron mobility decrease as a result of the shift in Fermi energy with respect to the graphene Dirac point, although the effect is partly compensated by a weaker electron−phonon coupling in the presence of the adlayer; the lowering in mobility is more pronounced for the electrons because of the presence around the Fermi level of an extra flat band associated with the acceptors that act as electron traps (at least at low coverage). However, the charge carrier mobility of the doped graphene remains substantial with a maximum loss of 1 order of magnitude compared to pristine graphene. Therefore, noncovalent functionalization appears as an effective way to nondestructively tune the electronic properties of graphene.

METHODS

The repeated-slab approach is adopted in our calculation where the molecular dopant is adsorbed on one side of graphene with a vacuum thickness of 17 Å. According to the sizes of molecular dopants, graphene supercells of $2\sqrt{3} * 3$, $4\sqrt{3} * 6$ and $3\sqrt{3} * 3$ are used for the adsorption of TCNE derivatives, HATCN derivatives, and TTF molecule, respectively. Unless stated otherwise, all calculations are performed within the Vienna ab initio simulation package (VASP)[32−34] using the Perdew−Burke−Ernzerhof (PBE)[35] exchange-correlation functional and a plane-wave basis set with an energy cutoff of 400 eV. Since the vdW interactions play an important role in noncovalent functionalization, the recently developed DFT including dispersion corrections (DFT-D) method is applied.[36] Due to the asymmetric adsorption of molecules on only one side of graphene, a dipole correction is applied.[30] The whole adsorbed system is optimized until the remaining atomic forces are smaller than 0.02 eV/Å. All the three-dimensional isodensity representations in our work are produced by XCrySDen.[37] In order to benchmark the method above, we carry out the calculation on graphite first. Our calculated lattice constants for graphite are a = 2.464 Å and c = 6.434 Å, which are in good agreement with the experimental values a = 2.462 Å and c = 6.710 Å.[38] In addition, the calculated adsorption energy of 5.517 kJ/mol/layer/atom for graphene interlayer interatoms almost coincidences with the experimental value 5.5 kJ/mol/layer/atom.[39] We therefore conclude that the PBE-D method properly reproduces graphene structure and energetics.

The Boltzmann transport equation has been applied to study the intrinsic carrier mobility of carbon allotrope materials, such as carbon nanotube (CNT),[40] graphene nanoribbon (GNR),[41,42] graphdiyne,[43,44] and graphene.[45] Perebeinos and co-workers have studied the electron−phonon scattering in semiconducting CNTs, and found that the scattering comes entirely from the acoustic phonons under low field.[46] Therefore, we only consider the acoustic phonon scattering process in carrier transport, which can be described by the DP theory and the corresponding relaxation time can be expressed as[31]

$$\frac{1}{\tau_\alpha(i,\boldsymbol{k})} = \frac{2\pi}{\hbar}\frac{k_B T E_1^{\,2}}{C}\sum_{\boldsymbol{k}'}\delta[\varepsilon_i(\boldsymbol{k}) - \varepsilon_i(\boldsymbol{k}')]\left[1 - \frac{v_\alpha(i,\boldsymbol{k}')}{v_\alpha(i,\boldsymbol{k})}\right]$$

dx.doi.org/10.1021/jz4010174 | J. Phys. Chem. Lett. 2013, 4, 2158−2165

where α is the direction of a weak external field. $\varepsilon_i(\boldsymbol{k})$ is the energy of the ith band at state $\boldsymbol{k}$, which can be easily obtained from the DFT calculations. The group velocity $v_\alpha(i,\boldsymbol{k})$ along α can be calculated as $v(i,\boldsymbol{k}) = \nabla\varepsilon_i(\boldsymbol{k})/\hbar$. C is the elastic constant and E_1 is the DP constant. In order to obtain C and E_1, the lattice vectors are stretched and compressed along α. By fitting the total energy with respective to the lattice change, C can be derived from $(E-E_0)/V_0 = C\,(\Delta l_\alpha/l_{\alpha 0})^2/2$. Here, E_0 and V_0 are the total energy and cell volume at equilibrium, and $l_{\alpha 0}$ and Δl_α are the equilibrium lattice constant and the lattice change along α. The DP constant is defined as $E_1 = \Delta\varepsilon/(\Delta l_\alpha/l_{\alpha 0})$, where $\Delta\varepsilon$ is the energy change due to Δl_α. Generally, we take the energy change at valence band maximum (VBM) and conduction band minimum (CBM) for hole and electron, respectively. Finally, the carrier mobility is written as

$$\mu_\alpha^{\mathrm{h(e)}} = \frac{e}{k_B T} \times \frac{\sum_{i\in \mathrm{VB(CB)}} \int \tau_\alpha(i,\boldsymbol{k}) v_\alpha^2(i,\boldsymbol{k}) \exp[\pm\varepsilon_i(\boldsymbol{k})/k_B T]\,\mathrm{d}\boldsymbol{k}}{\sum_{i\in \mathrm{VB(CB)}} \int \exp[\pm\varepsilon_i(\boldsymbol{k})/k_B T]\,\mathrm{d}\boldsymbol{k}}$$

where the plus (minus) is for hole (electron). The sum of bands runs over VB for hole and CB for electron, and the integral of states is over the Brillouin zone.

■ ASSOCIATED CONTENT

Supporting Information

Figures S1−S5 and Table S1. This material is available free of charge via the Internet at http://pubs.acs.org.

■ AUTHOR INFORMATION

Corresponding Author

*E-mail: liping.chen@umons.ac.be.

Notes

The authors declare no competing financial interest.

■ ACKNOWLEDGMENTS

L.C. thanks Mr. Jinyang Xi and Dr. Ling Tang for the help in calculating the carrier mobility. This work has been supported by the European Science Foundation (ESF) under the EUROCORES Program EuroGRAPHENE (GOSPEL) and the EC Marie-Curie ITN-GENIUS (PITN-GA-2010-264694), FNRS-FRFC, and the Interuniversity Attraction Pole program (P7/05) initiated by the Belgian Science Policy Office. D.B. is a FNRS Research Director.

■ REFERENCES

(1) Novoselov, K. S.; Geim, A. K.; Morozov, S. V.; Jiang, D.; Zhang, Y.; Dubonos, S. V.; Grigorieva, I. V.; Firsov, A. A. Electric Field Effect in Atomically Thin Carbon Films. *Science* **2004**, *306*, 666−669.

(2) Morozov, S. V.; Novoselov, K. S.; Katsnelson, M. I.; Schedin, F.; Elias, D. C.; Jaszczak, J. A.; Geim, A. K. Giant Intrinsic Carrier Mobilities in Graphene and Its Bilayer. *Phys. Rev. Lett.* **2008**, *100*, 016602.

(3) Schedin, F.; Geim, A. K.; Morozov, S. V.; Hill, E. W.; Blake, P.; Katsnelson, M. I.; Novoselov, K. S. Detection of Individual Gas Molecules Adsorbed on Graphene. *Nat. Mater.* **2007**, *6*, 652−655.

(4) Berger, C.; Song, Z. M.; Li, X. B.; Wu, X. S.; Brown, N.; Naud, C.; Mayou, D.; Li, T. B.; Hass, J.; Marchenkov, A. N. Electronic Confinement and Coherence in Patterned Epitaxial Graphene. *Science* **2006**, *312*, 1191−1196.

(5) Han, M. Y.; Özyilmaz, B.; Zhang, Y.; Kim, P. Energy Band-Gap Engineering of Graphene Nanoribbons. *Phys. Rev. Lett.* **2007**, *98*, 206805.

(6) Zhang, Y.; Tang, T.-T.; Girit, C.; Hao, Z.; Martin, M. C.; Zettl, A.; Crommie, M. F.; Shen, Y. R.; Wang, F. Direct Observation of a Widely Tunable Bandgap in Bilayer Graphene. *Nature* **2009**, *459*, 820−823.

(7) Novoselov, K. S.; McCann, E.; Morozov, S. V.; Fal'ko, V. I.; Katsnelson, M. I.; Zeitler, U.; Jiang, D.; Schedin, F.; Geim, A. K. Unconventional Quantum Hall Effect and Berry's Phase of 2π in Bilayer Graphene. *Nat. Phys.* **2006**, *2*, 177−180.

(8) Liu, H.; Liu, Y.; Zhu, D. Chemical Doping of Graphene. *J. Mater. Chem.* **2011**, *21*, 3335−3345.

(9) Georgakilas, V.; Otyepka, M.; Bourlinos, A. B.; Chandra, V.; Kim, N.; Kemp, K. C.; Hobza, P.; Zboril, R.; Kim, K. S. Functionalization of Graphene: Covalent and Non-covalent Approaches, Derivatives and Applications. *Chem. Rev.* **2012**, *112*, 6156−6214.

(10) Chen, J. H.; Jang, C.; Adam, S.; Fuhrer, M. S.; Williams, E. D.; Ishigami, M. Charged-Impurity Scattering in Graphene. *Nat. Phys.* **2008**, *4*, 377−381.

(11) Panchokarla, L. S.; Subrahmanyam, K. S.; Saha, S. K.; Govindaraj, A.; Krishnamurthy, H. R.; Waghmare, U. V.; Rao, C. N. R. Synthesis, Structure, and Properties of Boron- and Nitrogen-Doped Graphene. *Adv. Mater.* **2009**, *21*, 4726−4730.

(12) Wei, D.; Liu, Y.; Wang, Y.; Zhang, H.; Huang, L.; Yu, G. Synthesis of N-Doped Graphene by Chemical Vapor Deposition and Its Electrical Properties. *Nano Lett.* **2009**, *9*, 1752−1758.

(13) Elias, D. C.; Nair, R. R.; Mohiuddin, T. M. G.; Morozov, S. V.; Blake, P.; Halsall, M. P.; Ferrari, A. C.; Boukhvalov, D. W.; Katsnelson, M. I.; Geim, A. K.; Novoselov, K. S. Control of Graphene's Properties by Reversible Hydrogenation: Evidence for Graphane. *Science* **2009**, *323*, 610−613.

(14) Boukhvalov, D. W.; Katsnelson, M. I. Chemical Functionalization of Graphene. *J. Phys.: Condens. Matter* **2009**, *21*, 344205.

(15) Bruzzone, S.; Fiori, G. Ab-Initio Simulations of Deformation Potentials and Electron Mobility in Chemically Modified Graphene and Two-Dimensional Hexagonal Boron-Nitride. *App. Phys. Lett.* **2011**, *99*, 222108.

(16) Chen, W.; Chen, S.; Qi, D. C.; Gao, X. Y.; Wee, A. T. S. Surface Transfer p-Type Doping of Epitaxial Graphene. *J. Am. Chem. Soc.* **2007**, *129*, 10418−10422.

(17) Voggu, R.; Das, B.; Rout, S. C.; Rao, C. N. R. Effects of Charge Transfer Interaction of Graphene with Electron Donor and Acceptor Molecules Examined Using Raman Spectroscopy and Cognate Techniques. *J. Phys.: Condens. Matter* **2008**, *20*, 472204.

(18) Sun, J. T.; Lu, Y. H.; Chen, W.; Feng, Y. P.; Wee, A. T. S. Linear Tuning of Charge Carriers in Graphene by Organic Molecules and Charge-Transfer Complexes. *Phys. Rev. B* **2010**, *81*, 155403.

(19) Manna, A. K.; Pati, S. K. Tuning the Electronic Structure of Graphene by Molecular Charge Transfer: A Computational Study. *Chem. Asian J.* **2009**, *4*, 855−860.

(20) Hu, T.; Gerber, I. C. Theoretical Study of the Interaction of Electron Donor and Acceptor Molecules with Graphene. *J. Phys. Chem. C* **2013**, *117*, 2411−2420.

(21) Lu, Y. H.; Chen, W.; Feng, Y. P.; He, P. M. Tuning the Electronic Structure of Graphene by an Organic Molecule. *J. Phys. Chem. B* **2009**, *113*, 2−5.

(22) Tian, X. Q.; Xu, J. B.; Wang, X. M. Band Gap Opening of Bilayer Graphene by F4-TCNQ Molecular Doping and Externally Applied Electric Field. *J. Phys. Chem. B* **2010**, *114*, 11377−11381.

(23) An edge-on configuration of HATCN on graphene is preferred at higher coverage, as indicated by the near edge X-ray absorption fine structure investigations of N. Koch and co-workers (unpublished results).

(24) Wang, L.; Rangger, G. M.; Romaner, L.; Heimel, G.; Bučko, T.; Ma, Z.; Li, Q.; Shuai, Z.; Zojer, E. Electronic Structure of Self-Assembled Monolayers on Au(111) Surfaces: The Impact of Backbone Polarizability. *Adv. Funct. Mater.* **2009**, *19*, 3766−3775.

(25) Ma, Z.; Rissner, F.; Wang, L.; Heimel, G.; Li, Q.; Shuai, Z.; Zojer, E. Electronic Structure of Pyridine-Based SAMs on Flat Au(111) Surfaces: Extended Charge Rearrangements and Fermi Level Pinning. *Phys. Chem. Chem. Phys.* **2011**, *13*, 9747−9760.

(26) Björk, J.; Stafström, S.; Hanke, F. Zipping Up: Cooperativity Drives the Synthesis of Graphene Nanoribbons. *J. Am. Chem. Soc.* **2011**, *133*, 14884−14887.
(27) Heyd, J.; Scuseria, G. E.; Ernzerhof, M. Hybrid Functionals Based on a Screened Coulomb Potential. *J. Chem. Phys.* **2003**, *118*, 8207−8215.
(28) Heyd, J.; Scuseria, G. E.; Ernzerhof, M. Erratum: "Hybrid Functionals Based on a Screened Coulomb Potential" [J. Chem. Phys. 118, 8207 (2003)]. *J. Chem. Phys.* **2006**, *124*, 219906.
(29) Paier, J.; Marsman, M.; Hummer, K.; Kresse, G.; Gerber, I. C.; Ángyán, J. G. Screened Hybrid Density Functionals Applied to Solids. *J. Chem. Phys.* **2006**, *124*, 154709.
(30) Makov, G.; Payne, M. C. Periodic Boundary Conditions in Ab Initio Calculations. *Phys. Rev. B* **1995**, *51*, 4014−4022.
(31) Bardeen, J.; Shockley, W. Deformation Potentials and Mobilities in Non-polar Crystals. *Phys. Rev.* **1950**, *80*, 72−80.
(32) Kresse, G.; Hafner, J. Ab Initio Molecular Dynamics for Liquid Metals. *Phys. Rev. B* **1993**, *47*, 558−561.
(33) Kresse, G.; Furthmüller, J. Efficient Iterative Schemes for Ab Initio Total-Energy Calculations Using a Plane-Wave Basis Set. *Phys. Rev. B* **1996**, *54*, 11169−11186.
(34) Kresse, G.; Furthmüller, J. Efficiency of Ab-Initio Total Energy Calculations for Metals and Semiconductors Using a Plane-Wave Basis Set. *Comput. Mater. Sci.* **1996**, *6*, 15−50.
(35) Perdew, J. P.; Burke, K.; Ernzerhof, M. Generalized Gradient Approximation Made Simple. *Phys. Rev. Lett.* **1996**, *77*, 3865−3868.
(36) Grimme, S. Semiempirical GGA-Type Density Functional Constructed with a Long-Range Dispersion Correction. *J. Comput. Chem.* **2006**, *27*, 1787−1799.
(37) Kokalj, A. Computer Graphics and Graphical User Interfaces As Tools in Simulations of Matter at the Atomic Scale. *Comput. Mater. Sci.* **2003**, *28*, 155−168.
(38) Tuinstra, F.; Koenig, J. L. Raman Spectrum of Graphite. *J. Chem. Phys.* **1970**, *53*, 1126.
(39) Zacharia, R.; Ulbricht, H.; Hertel, T. Interlayer Cohesive Energy of Graphite from Thermal Desorption of Polyaromatic Hydrocarbons. *Phys. Rev. B* **2004**, *69*, 155406.
(40) Xu, B.; Xia, Y. D.; Yin, J.; Wan, X. G.; Jiang, K.; Li, A. D.; Wu, D.; Liu, Z. G. The Effect of Acoustic Phonon Scattering on the Carrier Mobility in the Semiconducting Zigzag Single Wall Carbon Nanotubes. *App. Phys. Lett.* **2010**, *96*, 183108.
(41) Long, M.-Q.; Tang, L.; Wang, D.; Wang, L.; Shuai, Z. Theoretical Predictions of Size-Dependent Carrier Mobility and Polarity in Graphene. *J. Am. Chem. Soc.* **2009**, *131*, 17728−17729.
(42) Wang, J.; Zhao, R.; Yang, M.; Liu, Z.; Liu, Z. Inverse Relationship between Carrier Mobility and Bandgap in Graphene. *J. Chem. Phys.* **2013**, *138*, 084701.
(43) Long, M.; Tang, L.; Wang, D.; Li, Y.; Shuai, Z. Electronic Structure and Carrier Mobility in Graphdiyne Sheet and Nanoribbons: Theoretical Predictions. *ACS Nano* **2011**, *5*, 2593−2600.
(44) Chen, J.; Xi, J.; Wang, D.; Shuai, Z. Carrier Mobility in Graphyne Should Be Even Larger than That in Graphene: A Theoretical Prediction. *J. Phys. Chem. Lett.* **2013**, *4*, 1443−1448.
(45) Xi, J.; Long, M.; Tang, L.; Wang, D.; Shuai, Z. First-Principles Prediction of Charge Mobility in Carbon and Organic Nanomaterials. *Nanoscale* **2012**, *4*, 4348−4369.
(46) Perebeinos, V.; Tersoff, J.; Avouris, P. Electron-Phonon Interaction and Transport in Semiconducting Carbon Nanotubes. *Phys. Rev. Lett.* **2005**, *94*, 086802.